Modeling the excitation of guided waves in generally anisotropic multilayered media

Alexander Velichko[a] and Paul D. Wilcox[b]
Department of Mechanical Engineering, University of Bristol, Bristol, BS8 1TR, United Kingdom

(Received 1 May 2006; revised 16 October 2006; accepted 17 October 2006)

The design of transducers to excite and detect guided waves is a fundamental part of a nondestructive evaluation or structural health monitoring system and requires the ability to predict the radiated guided wave field of a transmitting transducer. For most transducers, this can be performed by making the assumption that the transducer is weakly coupled and then integrating the Green's function of the structure over the area of the transducer. The majority of guided wave modeling is based on two-dimensional (2D) formulations where plane, straight-crested waves are modeled. Several techniques can be readily applied to obtain the solution to the forced 2D problem in terms of modal amplitudes. However, for transducer modeling it is desirable to obtain the complete three-dimensional (3D) field, which is particularly challenging in anisotropic materials. In this paper, a technique for obtaining a far-field asymptotic solution to the 3D Green's function in terms of the modal solutions to the forced 2D problem is presented. Results are shown that illustrate the application of the technique to isotropic (aluminium) and anisotropic (cross-ply and unidirectional composite) plates. Where possible, results from the asymptotic model are compared to those from 3D time-marching finite element simulations and good agreement is demonstrated.
 [DOI: 10.1121/1.2390674]

PACS number(s): 43.20.Bi, 43.35.Cg, 43.35.Zc [RMW] Pages: 60–69

I. INTRODUCTION

The analysis of guided waves in multilayered media has been the subject of a considerable amount of research for over a century. The first solutions of the unforced modal problem considered a two-dimensional (2D) cross section through the waveguide. In this formulation, the media are assumed to be in a state of plane strain and the guided wave modes predicted are plane, straight-crested waves with wave fronts perpendicular to the cross section. In the current paper, the plane-strain formulation for straight-crested guided waves is referred to as the 2D formulation. Much research has been devoted to analyzing the dispersion relationships for guided waves using the 2D formulation and a number of methods of solution have been developed including global and transfer matrix methods[1–3] and semianalytical finite element (SAFE) methods.[4,5] Numerical solutions using some of these methods are well established and commercially available.[6] Although less well known, the tools for predicting the amplitude of excited guided waves based on a 2D formulation are also well established. For example, the forced problem can be solved directly by using integral transforms,[7–9] the SAFE method[10] or by using modal expansion and the principle of reciprocity.[11,12]

In practice the modal solution obtained from a 2D formulation provides an adequate basis for understanding many aspects of wave propagation in real three-dimensional (3D) structures. However, the 2D formulation is a much less satisfactory basis for modeling the radiated guided wave field from a finite sized transducer, since the 2D formulation inherently requires the force distribution to extend infinitely in the plane perpendicular to the cross section. To accurately model a transducer a 3D formulation is required. This has been addressed by a number of researchers for specific cases. There are several approaches to finding the solution of the 3D forced problem. For example, the 3D wave field due to surface load can be calculated by using multiple integral transforms coupled with matrix methods for isotropic[13] and anisotropic[14] materials or using a modal expansion method.[15] It is also possible to use the finite element method[16] or other numerical methods.[17] In some particular cases the analytical expressions for the 3D solutions can be obtained. For example, for an isotropic plate and axisymmetric normal surface loading such formulas have been presented by Ditri *et al.*[18]

In this paper, the 3D Green's function is written in such a way that its far-field asymptotic solution can be expressed in terms of the modal expansion of a forced 2D system, which, as previously noted, can be obtained by a number of established methods. A technique is therefore provided for numerically computing the 3D excited guided wave field from a finite sized transducer using only the dispersion relationships and mode shapes obtained from 2D formulations. For the case of an isotropic plate such a method has been presented by Wilcox.[19] In the recent paper by Moulin *et al.*[20] the particular case of normal surface force on the isotropic plate is considered. Based on existing analytical expressions for solutions to the 3D and 2D problems, the authors then derived the relationship between them. However, analytical solutions are available for only a few specific cases, and direct comparison between 3D and 2D solutions becomes impossible for the case of anisotropic layered media. The

[a]Author to whom correspondence should be addressed. Electronic mail: a.velichko@bristol.ac.uk
[b]Electronic mail: p.wilcox@bristol.ac.uk

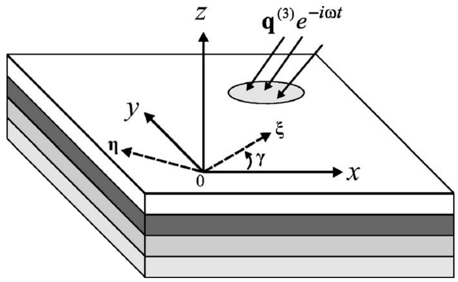

FIG. 1. System geometry.

technique proposed here is applicable to generally anisotropic layered media, although the relationship between 2D and 3D solutions is more complex than in isotropic or transversely isotropic layered media.

II. THEORY

A. Formulation of general 3D problem

A planar multilayered system consisting of N generally anisotropic layers is considered with Cartesian coordinate axes (x,y,z) defined with the z axis normal to the plane of the layers. An arbitrary time harmonic load $\mathbf{q}^{(3)}\ e^{-i\omega t}$ is applied to the upper surface of the system at $z=0$. The system is illustrated schematically in Fig. 1. The resulting time-harmonic displacement field in the system due to $\mathbf{q}^{(3)}$ is denoted by $\mathbf{u}^{(3)}$. The function $\mathbf{u}^{(3)}$ is related to $\mathbf{q}^{(3)}$ by the 3D Green's function $\mathbf{g}^{(3)}(x,y,z)$:

$$\mathbf{u}^{(3)}(x,y,z,\mathbf{q}^{(3)}) = \int\int \mathbf{g}^{(3)}(x-x',y-y',z) \times\mathbf{q}^{(3)}(x',y')dx'dy'. \quad (1)$$

The Green's function, $\mathbf{g}^{(3)}$, can be written in terms of its 2D spatial Fourier transform, $\mathbf{G}^{(3)}$, as

$$\mathbf{g}^{(3)}(x,y,z) = \frac{1}{4\pi^2}\int\int \mathbf{G}^{(3)}(k_x,k_y,z)e^{i(k_x x+k_y y)}dk_x dk_y, \quad (2)$$

where the matrix $\mathbf{G}^{(3)}(k_x,k_y,z)$ is the Green's function for straight-crested waves propagating in the direction given by the components k_x,k_y of the wave vector.

B. 2D problem

A new coordinate system (ξ,η,z) is defined that is a rotation of the original coordinate system by an angle γ about the vertical axis z (Fig. 1).

A special case of $\mathbf{q}^{(3)}$ may be defined as $\mathbf{q}^{(2)}(\xi)$ which is invariant in the η direction. The displacement field due to this loading is defined as $\mathbf{u}^{(2)}(\gamma,\xi,z,\mathbf{q}^{(2)})$. The loading $\mathbf{q}^{(2)}$ and displacement $\mathbf{u}^{(2)}$ represent the case of 2D excitation. The relationship between $\mathbf{u}^{(2)}$ and $\mathbf{q}^{(2)}$ may be written as the convolution integral

$$\mathbf{u}^{(2)}(\gamma,\xi,z,\mathbf{q}^{(2)}) = \int \mathbf{g}^{(2)}(\gamma,\xi-\xi',z)\mathbf{q}^{(2)}(\xi')d\xi', \quad (3)$$

where $\mathbf{g}^{(2)}$ is the 2D Green's function; $\mathbf{g}^{(2)}$ can be written in terms of its one-dimensional spatial Fourier transform, $\mathbf{G}^{(2)}$, as

$$\mathbf{g}^{(2)}(\gamma,\xi,z) = \frac{1}{2\pi}\int_{-\infty}^{+\infty} \mathbf{G}^{(2)}(\gamma,k,z)e^{ik\xi}dk. \quad (4)$$

By using the residues technique, the integration in Eq. (4) can be reduced to the sum of residuals

$$\mathbf{g}^{(2)}(\gamma,\xi,z) = \sum_m \mathbf{E}_m^{(2)}(\gamma,z)e^{ik_m\xi},$$

$$\mathbf{E}_m^{(2)}(\gamma,z) = i \text{ res } \mathbf{G}^{(2)}(\gamma,k,z)\big|_{k=k_m}, \quad (5)$$

where $\mathbf{E}_m^{(2)}$ is defined as the 2D modal excitability matrix.

The real poles of the matrix $\mathbf{G}^{(2)}$ represent the propagating waves while the complex poles represent nonpropagating waves that decay exponentially with propagation distance from the source. In this paper only the contributions from real poles are considered.

To solve the 2D problem using the described integral transforms method it is necessary to calculate matrix $\mathbf{G}^{(2)}$. The modal solution of the forced 2D problem can also be obtained by a number of other established methods. For example, the reciprocity approach[11] leads to an alternative expression for mode amplitude $\mathbf{E}_m^{(2)}$ that is useful because it can be computed directly from the mode shape. The expression for propagating mode amplitude (see, for example, Núñez *et al.*[21]) is

$$\mathbf{E}_m^{(2)}(\gamma,z) = \frac{i\omega}{4P_m}\mathbf{u}_m(\gamma,z)\cdot\mathbf{u}_m^{*T}(\gamma,z=0), \quad (6)$$

where * denotes complex conjugation, T represents transpose and $\mathbf{u}_m=(u_{mx},u_{my},u_{mz})^T$ is the displacement field distribution for mth mode. Coefficient P_m is the average power flow of the mode, given by[11]

$$P_m = \frac{\omega}{2}\,\mathrm{Im}\int (\mathbf{T}_m\mathbf{u}_m^*)\mathbf{n}dz, \quad (7)$$

where $\mathbf{T}_m$ is the stress tensor and $\mathbf{n}=(1,0,0)^T$ is the direction of mode propagation.

C. Relation between 2D and 3D problems for straight-crested waves

Consider now the relationship between 2D and 3D Green's functions for straight-crested waves $\mathbf{G}^{(2)}$ and $\mathbf{G}^{(3)}$.

The transformation from the coordinate system (x,y,z) to the new coordinate system (ξ,η,z) is represented by the matrix $\mathbf{A}$

$$\begin{pmatrix}\xi\\ \eta\\ z\end{pmatrix} = \mathbf{A}(\gamma)\begin{pmatrix}x\\ y\\ z\end{pmatrix}, \quad \mathbf{A}(\gamma) = \begin{pmatrix}\cos\gamma & \sin\gamma & 0\\ -\sin\gamma & \cos\gamma & 0\\ 0 & 0 & 1\end{pmatrix}. \quad (8)$$

The Fourier variables, k_ξ and k_η, in the new coordinate system are related to those in the original coordinate system by

$$k_x = k_\xi\cos\gamma - k_\eta\sin\gamma, \quad k_y = k_\xi\sin\gamma + k_\eta\cos\gamma \quad (9)$$

The Green's matrix in the Fourier domain, $\mathbf{G}^{(3)}\times(k_x,k_y,z)$, is transformed as

$$\mathbf{G}_\gamma^{(3)}(k_\xi,k_\eta,z) = \mathbf{A}\mathbf{G}^{(3)}(k_\xi \cos\gamma - k_\eta \sin\gamma, k_\xi \sin\gamma + k_\eta \cos\gamma, z)\mathbf{A}^{-1}. \qquad (10)$$

Here $\mathbf{G}_\gamma^{(3)}(k_\xi,k_\eta,z)$ is the Green's function for straight-crested wave with wave vector $(k_\xi,k_\eta,0)$. On the other hand, $\mathbf{G}^{(2)}(\gamma,k,z)$ is Green's function for straight-crested wave with wave vector $(k,0,0)$. Hence,

$$\mathbf{G}^{(2)}(\gamma,k,z) = \mathbf{G}_\gamma^{(3)}(k,0,z),$$

or

$$\mathbf{G}^{(2)}(\gamma,k,z) = \mathbf{A}\mathbf{G}^{(3)}(k\cos\gamma, k\sin\gamma, z)\mathbf{A}^{-1}. \qquad (11)$$

D. Far-field asymptotic solution to 3D problem

The double wave number integral (2) can be evaluated numerically and different calculation methods have been developed.[22,23] But numerical evaluation of this type of integral is very difficult due to the presence of singularities and the high oscillation of integrand in the far-field zone. An alternative approach is asymptotical analysis of the integral, which is used in this paper.

Expression (5) gives the expansion of the 2D solution in terms of 2D modes. In this section the analogous mode expansion of the 3D solution in the far-field will be derived. As in the 2D case the mode amplitudes are proportional to the residuals for real poles of the matrix $\mathbf{G}^{(3)}$. Then by using Eq. (11) it is possible to obtain the relationship between mode amplitudes in 2D and 3D cases.

First a change of global coordinates from Cartesian (x,y,z) to cylindrical polar (r,φ,z) is defined:

$$x = r\cos\varphi, \quad y = r\sin\varphi, \quad k_x = k\cos\gamma, \quad k_y = k\sin\gamma.$$

The expression (2) for the 3D Green's function $\mathbf{g}^{(3)}$ can therefore be written in (r,φ,z) coordinates as:

$$\mathbf{g}^{(3)}(r,\varphi,z) = \frac{1}{4\pi^2}\int_{\varphi-\pi/2}^{\varphi+3\pi/2}\int_\Gamma \mathbf{G}^{(3)}(k\cos\gamma,\ k\sin\gamma, z) \times e^{ikr\cos(\gamma-\varphi)} k\,dk\,d\gamma. \qquad (12)$$

The contour of integration Γ coincides with the real positive half axis except for real poles. In these points it diverges in the complex plane k in accordance with the principle of limiting absorption.[7,13]

The integral with respect to γ is divided into two parts: from $\varphi-\pi/2$ to $\varphi+\pi/2$ and from $\varphi+\pi/2$ to $\varphi+3\pi/2$. In the second integral γ is changed to $\gamma+\pi$ and k to $-k$. Then

$$\mathbf{g}^{(3)}(r,\varphi,z) = \frac{1}{4\pi^2}\int_{\varphi-\pi/2}^{\varphi+\pi/2}\int_{\Gamma\cup-\Gamma} \mathbf{G}^{(3)}(k\cos\gamma,\ k\sin\gamma, z) \times e^{ikr\cos(\gamma-\varphi)} k\,dk\,d\gamma. \qquad (13)$$

The integration with respect to k can be performed by using the residues theory. The contours Γ and $-\Gamma$ can be closed in the upper half plane of k and the integrals are reduced to the sum of residues of the poles and integrals along the imaginary axis. Propagating modes are described by the real poles only and decrease as $r^{-1/2}$ as $r\to\infty$. The contributions of the residues in complex poles and integrals along the imaginary axis have a larger order of decrease. Therefore,

$$\mathbf{g}^{(3)} = \frac{1}{2\pi}\sum_m \int_{\varphi-\pi/2}^{\varphi+\pi/2} \mathbf{G}_m^{(3)}(\gamma,z)|k_m(\gamma)| e^{ik_m(\gamma) r\cos(\gamma-\varphi)} d\gamma + O(r^{-3/2}), \quad r\to\infty,$$

$$\mathbf{G}_m^{(3)}(\gamma,z) = i \operatorname{res} \mathbf{G}^{(3)}(k\cos\gamma, k\sin\gamma, z)\big|_{k=k_m(\gamma)}. \qquad (14)$$

Integrals with respect to γ are then calculated using the stationary phase method. This enables the final expression for the far-field asymptote to the 3D problem to be written as:

$$\mathbf{g}^{(3)}(r,\varphi,z) = \frac{1}{\sqrt{r}}\sum_m \mathbf{E}_m^{(3)}(\varphi,z)e^{ir\Phi_m(\gamma_m,\varphi)} + O(r^{-3/2}), \quad r\to\infty,$$

$$\mathbf{E}_m^{(3)}(\varphi,z) = B_m(\varphi)\mathbf{G}_m^{(3)}(\gamma_m,z), \qquad (15)$$

where $\mathbf{E}_m^{(3)}$ is defined as the 3D modal excitability matrix.

The phase functions Φ_m and coefficients B_m are given by

$$\Phi_m(\gamma,\varphi) = k_m(\gamma)\cos(\gamma-\varphi),$$

$$B_m = \frac{|k_m(\gamma_m)|}{\sqrt{2\pi|b_m|}}\exp\left\{i\frac{\pi}{4}\operatorname{sgn} b_m\right\}, \quad b_m = \frac{\partial^2\Phi_m(\gamma_m,\varphi)}{\partial\gamma^2}. \qquad (16)$$

The angle $\gamma_m \equiv \gamma_m(\varphi)$ is found from the following equation:

$$\frac{\partial\Phi_m(\gamma,\varphi)}{\partial\gamma} = 0, \quad \varphi - \frac{\pi}{2} \le \gamma \le \varphi + \frac{\pi}{2}. \qquad (17)$$

The angles φ and γ_m are related by

$$\varphi = \gamma_m + \arctan\frac{c'(\gamma_m)}{c(\gamma_m)}, \qquad (18)$$

here $c(\gamma) = \omega / k_m(\gamma)$ is phase velocity.

E. Relation between 2D and 3D problems

In summary, the 2D Green's function is

$$\mathbf{g}^{(2)}(\gamma,\xi,z) = \sum_m \mathbf{E}_m^{(2)}(\gamma,z)e^{ik_m\xi},$$

and the far-field asymptotic to the 3D Green's function is

$$\mathbf{g}^{(3)}(r,\varphi,z) = \frac{1}{\sqrt{r}}\sum_m \mathbf{E}_m^{(3)}(\varphi,z)e^{ir\Phi_m(\gamma_m,\varphi)}.$$

Using expression (11), the modal excitability matrices in the 2D and 3D cases can be related by

$$\mathbf{E}_m^{(3)}(\varphi,z) = B_m(\varphi)\mathbf{A}^{-1}(\gamma_m)\mathbf{E}_m^{(2)}(\gamma_m,z)\mathbf{A}(\gamma_m). \qquad (19)$$

The far-field solution for a particular mode in the φ direction is therefore intimately related to the appropriate 2D solution for the same mode in the γ_m direction.

The phase function Φ_m can be written as $\Phi_m = \mathbf{k}_m \cdot \mathbf{n}$. In this expression $\mathbf{k}_m = (k_m(\gamma_m)\cos\gamma_m, k_m(\gamma_m)\sin\gamma_m)^T$ is a wave

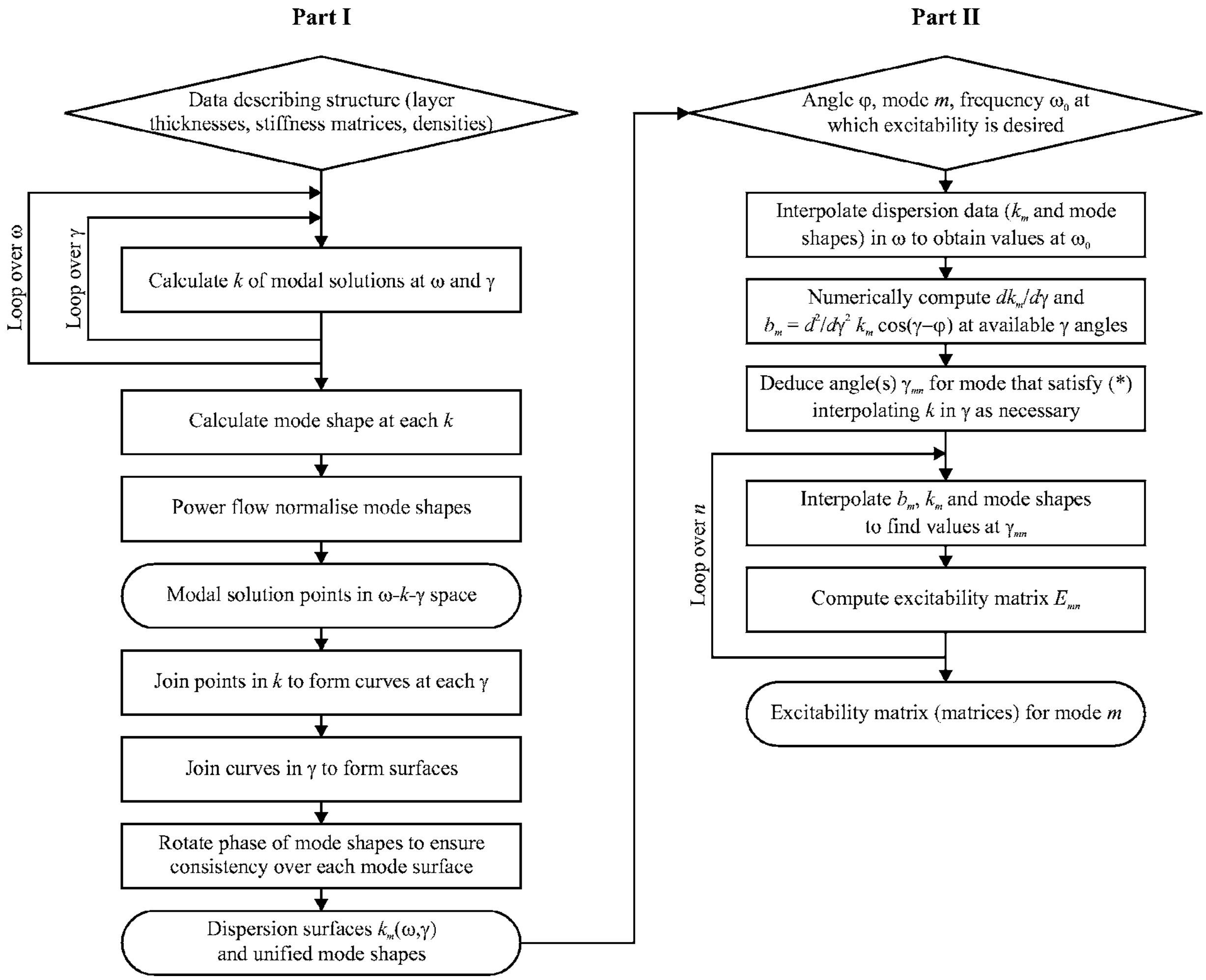

FIG. 2. Flow chart of excitability calculation.

vector and $\mathbf{n}=(\cos\varphi,\sin\varphi)^T$ is a unit vector in φ direction. Therefore, the angle(s) γ_m is the phase velocity direction(s) for the mth mode. Moreover, the relation (18) shows that vector $\mathbf{n}$ is normal to the slowness surface, $\mathbf{k}_m(\gamma)/\omega$, at the direction γ_m. It means that angle φ is direction of group velocity for the mth mode.[11]

Note that the coefficients b_m in expression (16) can be written in the form

$$b_m = -\frac{\omega}{c\sqrt{c^2+(c')^2}}(c''+c)\bigg|_{\gamma=\gamma_M}. \tag{20}$$

It is supposed in the previous analysis that $b_m \neq 0$. From Eq. (18) we obtain that if $b_m=0$, then $d\varphi/d\gamma=0$. In this case the group velocity direction remains the same while the phase velocity direction varies and in such directions the wave field decays as $O(r^{-1/3})$.

The complete procedure for predicting the far-field displacement in the φ direction under point harmonic loading is as follows:

- Compute dispersion relationships $k_m(\gamma)$. For mth mode, find angle or angles γ_m.
- Solve 2D problem at angle γ_m.
- Compute the amplitude of 3D mode at angle φ from 2D solution at angle γ_m.

In the special case of an isotropic or transversely isotropic layered medium, the slowness profiles of all modes are circular, hence the phase and group velocity directions are identical. In this case, the relationship between 2D and 3D modal excitability matrices reduces to

$$\mathbf{E}_m^{(3)}(\varphi,z) = \sqrt{\frac{k_m}{2\pi}}e^{-i\pi/4}\mathbf{A}^{-1}(\varphi)\mathbf{E}_m^{(2)}(z)\mathbf{A}(\varphi). \tag{21}$$

In the case of material damping all wave numbers k_m become complex and the asymptotic of the solution given by Eq. (15) to the 3D problem is not valid. This topic requires further research.

III. IMPLEMENTATION OF ASYMPTOTIC MODEL

The asymptotic model described in the previous section has been implemented numerically using functions written in the MATLAB (The Mathworks Inc., Natick, Massachusetts) modeling environment. The overall operation of the numerical program is shown in the flow chart in Fig. 2, and can be separated into two distinct parts. The first part of the program generates dispersion data for the structure and the second part converts this into modal excitability matrices for guided wave propagation in a specified direction.

A. Dispersion curve generation

Dispersion curves are generated for different angles of propagation using a semianalytic finite element technique (implemented in MATLAB) similar to that described by Hayashi, Song, and Rose.[5] Other dispersion curve calculation techniques such as the global matrix or transfer matrix methods[2] could also be used. The semianalytic finite element method is used here to allow easy integration of the complete model in MATLAB. For each angle, γ, this technique yields a number of discrete points lying in ω-k space, where k is complex. Each point corresponds to a modal solution for the propagation of straight-crested guided waves in the γ direction. Associated with each point is a displacement mode shape, from which the stress mode shape and hence the power flow associated with any chosen amplitude of wave can be deduced. At this stage the mode shape at each point is power-flow normalized and points with imaginary k components are discarded as these correspond to nonpropagating modes. The result is a number of discrete points lying in $\omega - k - \gamma$ space and a power-flow normalized mode shape associated with each point.

The most challenging aspect of the numerical implementation is to link the discrete points in ω-k-γ space together into modes to create dispersion surfaces. This is required since it is necessary in the subsequent excitability calculation to interpolate modal data in both ω and γ and also to differentiate the wave number, k, of a mode with respect to γ [Eq. (17)]. First, points are linked at each γ angle by comparing the mode shapes at nearby points in ω-k space to form dispersion curves. Next, dispersion curves are linked between adjacent γ angles to form dispersion surfaces by comparing both mode shapes and dispersion curve shapes.

This aspect of the model is illustrated by the example in Fig. 3 which shows (a) the discrete points generated by the semianalytical finite element method and (b) the dispersion surfaces for three modes obtained by joining the points. For clarity the data in this figure have been plotted as phase-velocity rather then wave number versus frequency and angle. The dispersion data are for the cross-ply composite plate example discussed in the next section.

The final stage of the generation of dispersion data is to rotate the phase of mode shapes for each mode so that the phase is consistent at all points. This is necessary for subsequent interpolation between mode shapes of a mode in both ω and γ. The phase of mode shapes for all points on a mode are rotated so that the phase of the dominant surface component of the displacement mode shape is zero.

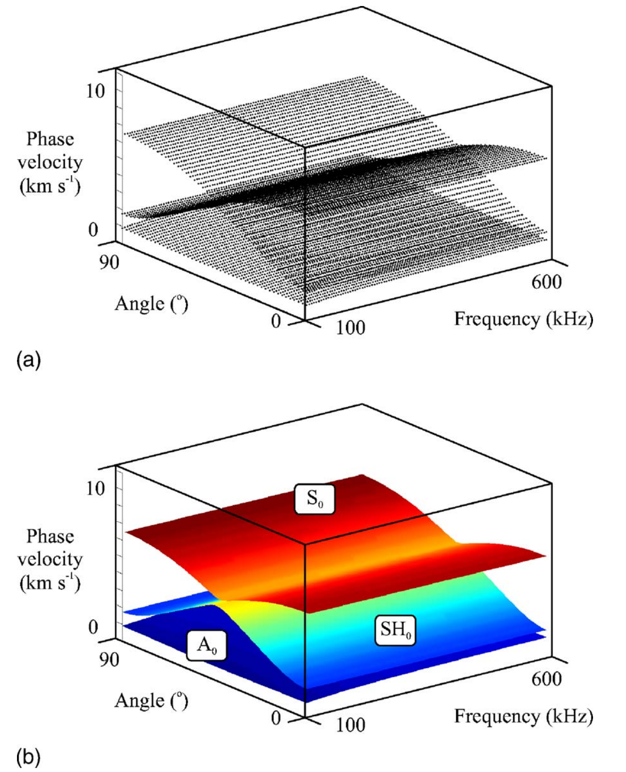

FIG. 3. (Color online) Example of dispersion data: (a) discrete points generated by the semianalytical finite element method and (b) the resulting dispersion surfaces. The data are for a cross-ply composite plate.

B. Excitability matrix calculation

Once the dispersion data are obtained for all modes, excitability matrices for any mode, m, frequency, ω_0, and propagation direction, φ, can be computed. First, the dispersion data (power flow normalized mode shape and wave number) are interpolated in ω to find its values at ω_0. The next stage of the calculation is to compute the angle or angles, γ_{mn}, which satisfy Eq. (17) for the mth mode in the φ direction. To perform this calculation, it is first necessary to numerically compute the derivatives $d/d\gamma\ [k_m(\omega_0,\gamma)]$ and $d^2/d^2\gamma\ [k_m(\omega_0,\gamma)\ \cos(\gamma-\varphi)]$. The first of these two quantities is used to identify pairs of discrete γ angles at which the available dispersion data bracket solutions to Eq. (18). Approximations to solutions γ_{mn} are obtained by linear interpolation between these angles. If there is more than one γ_{mn}, then each must be treated separately, and in the final result this effect appears as extra modes. The dispersion data and $d^2/d^2\gamma[k_m(\omega_0,\gamma)\cos(\gamma-\varphi)]$ are then interpolated again, this time in γ, to obtain values at γ_{mn}. The 2D excitability matrix, $\mathbf{E}_{mn}^{(2)}(\omega_0,\gamma_{mn})$, is calculated by using expression (6). Finally, the 3D excitability matrix, $\mathbf{E}_{mn}^{(3)}(\omega_0,\varphi)$, is computed according to Eq. (19) and the effective wave number in the φ direction, Φ_{mn}, is calculated from Eq. (16).

The excitability matrix and effective wave number provide all information necessary to perform wave excitation simulation. Typically this may involve the simulation of either time-domain signals recorded at a particular point or the surface displacement around a source at a particular instant in time.

IV. FINITE ELEMENT MODELING

In order to validate the implementation of the three-dimensional (3D) excitability model described in the previous sections, a number of explicit time marching finite element (FE) simulations have been performed. These are also 3D and require considerable computational power. Symmetry conditions are exploited where possible, but in order to distinguish different modes and separate directly excited modes from edge reflections, a significant area of a plate-like structure must be modeled. The maximum size of FE model

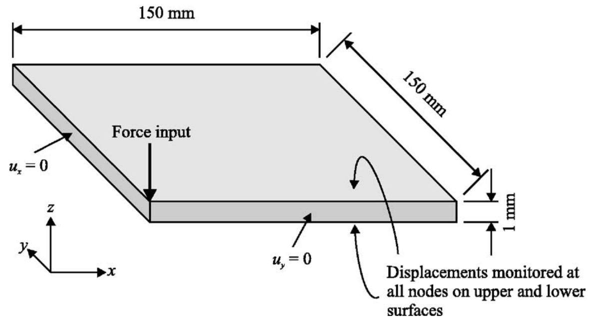

FIG. 4. Finite element (FE) model geometry.

that can be run on the computer resources available is limited to around 5×10^6 degrees of freedom and this means that a compromise must be made between the size of the structure modeled and the mesh density. For this reason, the mesh density used is somewhat less than ideal and this is manifested in an underestimate of guided wave velocity that is more pronounced for short wavelength modes. Notwithstanding these limitations, the FE results are sufficient to qualitatively show that the excitability algorithm has been correctly implemented and also to indicate the regions where the asymptotic assumptions break down.

The general FE model geometry, used for all cases considered here, is shown in Fig. 4. Cubic eight noded elements are used with side length 0.25 mm. Planes of symmetry are assigned as shown and only the response to out-of-plane forcing is considered. The force in all cases is a five cycle Hanning windowed toneburst with a center frequency of 300 kHz. All FE modeling was performed using the ABAQUS package (Version 6.5.2, ABAQUS Inc., Providence, RI) running on a Viglen CL2000, using a single Intel Xeon 32 GHz processor incorporating 64 bit PCI with a Linux operating system and 8 GB random access memory.

For comparison purposes, the displacement field due to each mode should ideally be analyzed separately. However, while the asymptotic model can be used on a mode by mode basis, the FE model implicitly includes the contributions from all guided wave modes. A rudimentary method for partially separating the contributions from different modes in the FE model, which has been employed here, is to monitor displacements at nodes on both upper and lower surfaces of the plate. This then allows the contributions to be separated into those due to symmetric and antisymmetric nodes. In the relatively low frequency thickness regime where the modeling has been performed in this paper, only three fundamental mode types exist corresponding to A_0 and S_0 Lamb-type modes and a symmetric shear-horizontal *SH*-type mode, referred to as SH_0. The modal separation technique employed therefore allows complete separation of the A_0 mode but not of the S_0 and SH_0 modes.

V. RESULTS

The results from a number of sample cases are presented here, beginning with the simplest case of guided waves in an isotropic plate excited by an out-of-plane point force. This demonstrates the procedure and also highlights the limited accuracy of the FE model. The excitation of guided waves by an out-of-plane point force in two highly anisotropic plates is then considered to illustrate the capability and limitations of the asymptotic model. The final case demonstrates the application of the asymptotic model to in-plane forcing of an isotropic plate which produces a nonaxisymmetric guided wave field. In all cases, a 1-mm-thick plate is considered and the excitation signal is a five cycle Hanning windowed toneburst with a center frequency of 300 kHz. At this frequency-thickness product the only propagating modes in all cases are the two fundamental Lamb modes (A_0 and S_0) and the fundamental shear-horizontal mode (SH_0). The reason for this choice of frequency-thickness product is to provide results that can be quantified and compared to FE results, it does not reflect any limitation of the asymptotic calculation. There is also no limitation other than increased mesh density and computation time in the semianalytic finite element method, although the subsequent connection of discrete dispersion points into dispersion surfaces becomes increasingly challenging if more modes are present.

TABLE I. Properties of aluminium plate

Property	Value	Units
Density	2700	kg m^{-3}
Young's modulus	70	MN mm^{-2}
Poisson's ratio	0.3	

A. Out-of-plane excitability of isotropic plate

The first case considered is an isotropic 1-mm-thick aluminium plate, the properties of which are shown in Table I. A_0, S_0 and SH_0 modes may exist in this system. However, the isotropy of the plate and orientation of the input force means that the problem is axisymmetric and hence only A_0 and S_0 are excited. Figures 5(a) and 5(b) show snapshots of the out-of-plane surface displacement 25 μs after the start of the input signal obtained from the FE model for the A_0 and S_0 modes. The nonaxisymmetric signal near the origin in Fig. 5(b) is due to the unwanted presence of higher order modes at the upper frequency limit of the input signal that cannot be correctly modeled by the mesh density used. Figures 5(c) and 5(d) show the equivalent results obtained from the asymptotic model. The gray scale in both images is the same, and it can be seen that the FE and asymptotic models are in excellent agreement. There is in fact a slight velocity discrepancy for the A_0 mode due to the relatively coarse mesh used in the FE model.

B. Cross-ply composite plate

A cross-ply composite plate has been modeled using equivalent homogenous properties which are listed in Table II. Again over the frequency range considered A_0, S_0 and SH_0-type modes may exist in this system. However, it should be noted that, other than in the 0° and 90° directions the mode shapes of S_0 and SH_0 both contain displacement components in directions parallel and perpendicular to the direction of propagation, hence the designation of the mode names in these directions is ambiguous. However, this at-

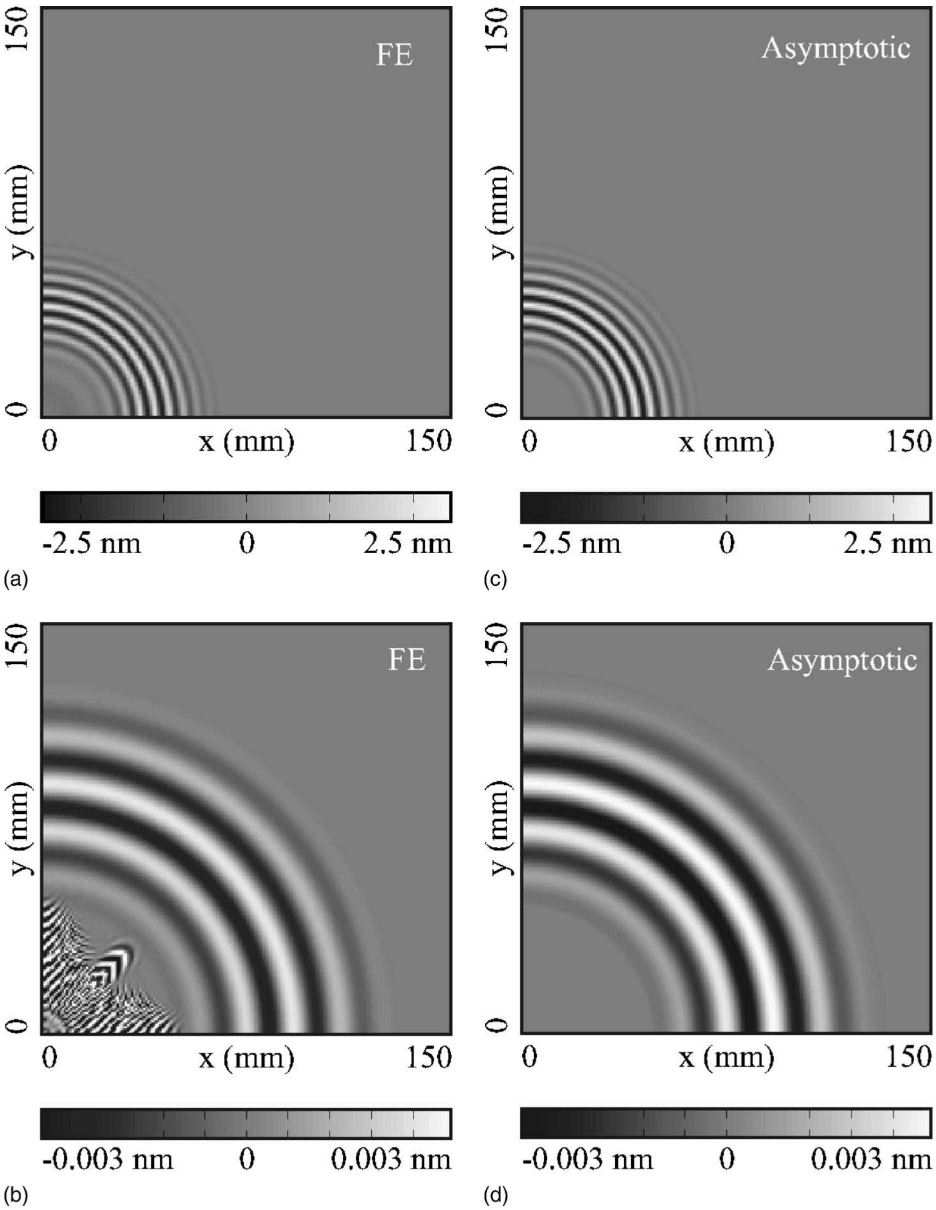

FIG. 5. Out-of-plane surface displacement of a 1-mm-thick aluminum plate, 25 μs after the start of a five cycle Hanning windowed toneburst of out-of-plane force applied at $(0,0)$ with center frequency 300 kHz: FE model results showing contributions from (a) A_0 mode and (b) S_0 mode; asymptotic model results showing contributions from (c) A_0 mode and (d) S_0 mode.

tribute of the mode shapes means that in this system, all three modes are excited by the application of an out-of-plane point force in certain directions.

Figures 6(a) and 6(b) show snapshots of the out-of-plane surface displacement 25 μs after the start of the input signal obtained from the FE model for the anti-symmetric (A_0) and symmetric modes (S_0 and SH_0), respectively. Figures 6(c) and 6(d) show the equivalent results obtained from the asymptotic model. Figures 6(e) and 6(f) show the results from the asymptotic model separated into contributions from the S_0 and SH_0 modes.

It can be seen that the FE and asymptotic models are in reasonable agreement with regard to the overall pattern of the radiated wave field and its amplitude. Of particular interest here is the behavior of the SH_0 mode. The latter has a highly anisotropic velocity profile and over the range of

TABLE II. Properties of cross-ply composite plate.

Property	Value						Units
Density	1560						kg m^{-3}
Stiffness matrix							
$c_{11},c_{12},c_{13},c_{14},c_{15},c_{16}$	64.24	5.6	7.73	0	0	0	MN mm^{-2}
$c_{21},c_{22},c_{23},c_{24},c_{25},c_{26}$	5.6	70.78	8.39	0	0	0	MN mm^{-2}
$c_{31},c_{32},c_{33},c_{34},c_{35},c_{36}$	7.73	8.39	13.3	0	0	0	MN mm^{-2}
$c_{41},c_{42},c_{43},c_{44},c_{45},c_{46}$	0	0	0	2.97	0	0	MN mm^{-2}
$c_{51},c_{52},c_{53},c_{54},c_{55},c_{56}$	0	0	0	0	3.06	0	MN mm^{-2}
$c_{61},c_{62},c_{63},c_{64},c_{65},c_{66}$	0	0	0	0	0	4.7	MN mm^{-2}

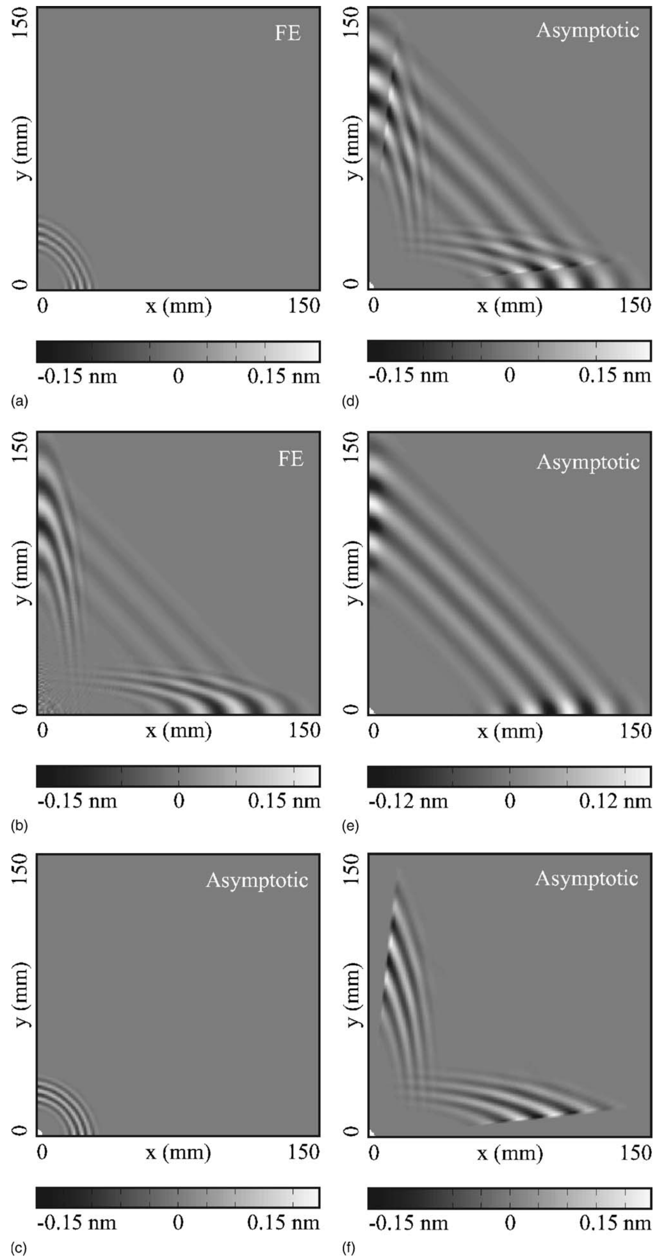

FIG. 6. Out-of-plane surface displacement of a 1-mm-thick cross-ply composite plate, 25 μs after the start of a five cycle Hanning windowed toneburst of out-of-plane force applied at $(0,0)$ with center frequency 300 kHz: FE model results showing contributions from (a) A_0 mode and (b) S_0+SH_0 modes; asymptotic model results showing contributions from (c) A_0 mode, (d) S_0+SH_0 modes, (e) S_0 mode and (f) SH_0 mode.

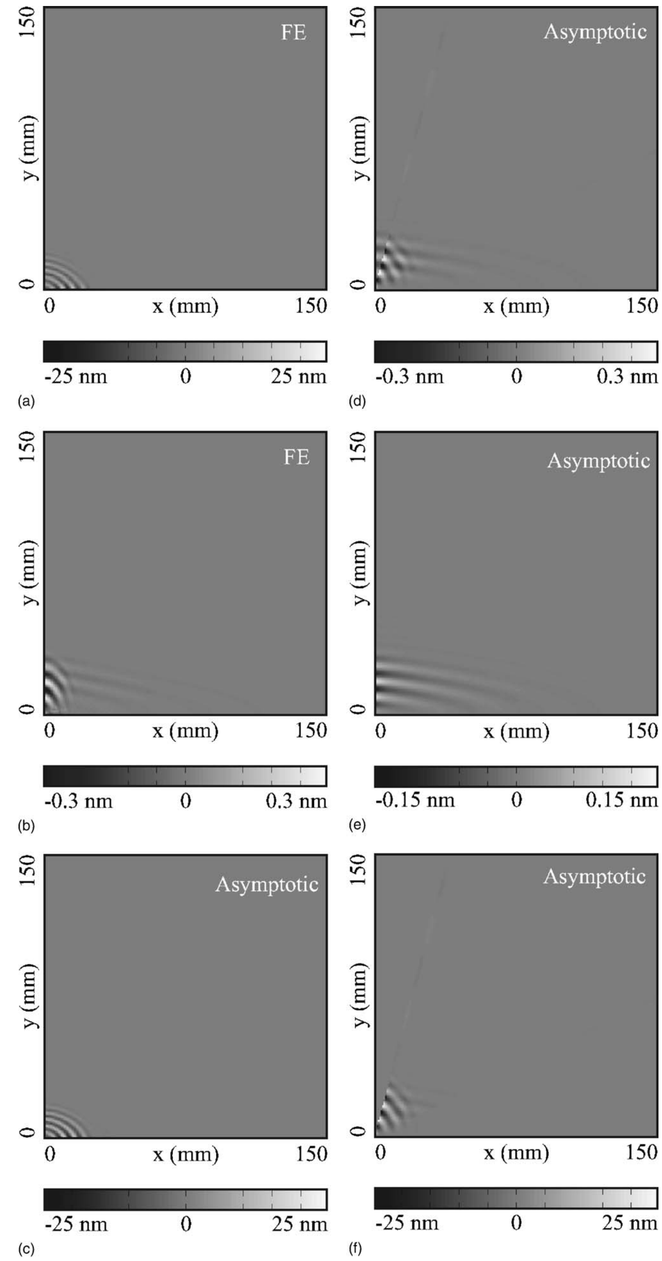

FIG. 7. Out-of-plane surface displacement of a 1-mm-thick uni-directional composite plate, 25 μs after the start of a five cycle Hanning windowed toneburst of out-of-plane force applied at $(0,0)$ with center frequency 300 kHz: FE model results showing contributions from (a) A_0 mode and (b) S_0+SH_0 modes; asymptotic model results showing contributions from (c) A_0 mode, (d) S_0+SH_0 modes, (e) S_0 mode and (f) SH_0 mode.

TABLE III. Properties of unidirectional composite plate

Property	Value						Units
Density	1560						kg m^{-3}
Stiffness matrix							
$c_{11},c_{12},c_{13},c_{14},c_{15},c_{16}$	143.8	6.2	6.2	0	0	0	MN mm^{-2}
$c_{21},c_{22},c_{23},c_{24},c_{25},c_{26}$	6.2	13.3	6.5	0	0	0	MN mm^{-2}
$c_{31},c_{32},c_{33},c_{34},c_{35},c_{36}$	6.2	6.5	13.3	0	0	0	MN mm^{-2}
$c_{41},c_{42},c_{43},c_{44},c_{45},c_{46}$	0	0	0	3.6	0	0	MN mm^{-2}
$c_{51},c_{52},c_{53},c_{54},c_{55},c_{56}$	0	0	0	0	3.6	0	MN mm^{-2}
$c_{61},c_{62},c_{63},c_{64},c_{65},c_{66}$	0	0	0	0	0	5.7	MN mm^{-2}

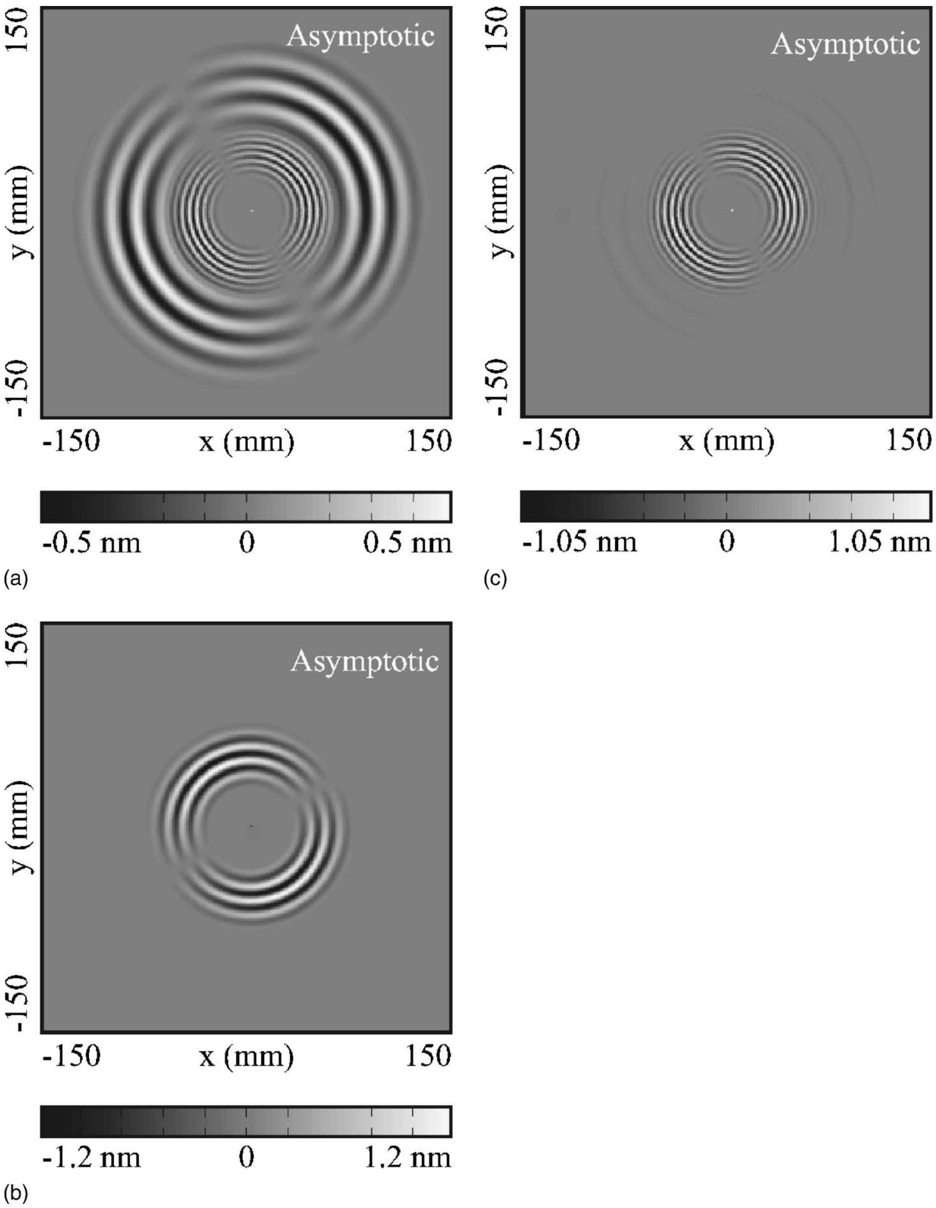

FIG. 8. Surface displacement of a 1-mm-thick aluminium plate, 25 μs after the start of a five cycle Hanning windowed toneburst of in-plane force applied at $(0,0)$ at 30º to horizontal with center frequency 300 kHz: (a) radial displacement, (b) angular displacement and (c) out-of-plane displacement.

propagation angles from 6 to 84° has three possible values of γ_{mn}, resulting in three different wave packets (the third and fastest SH_0 wave packet propagates with a similar profile to the S_0 mode but is of low amplitude and is scarcely visible in the figure). The velocity discrepancy between the models is particularly apparent for the slower SH_0 components around 45°. At the extremities of the angular range where the SH_0 modes exist, it can be seen that there is an abrupt discontinuity in displacements. This represents the breakdown of the asymptotic approximation in Eq. (15), since at these points the coefficient b_m in expression (16) is equal to zero and the group velocity direction is stationary.

C. Unidirectional composite plate

A uni-directional composite plate has also been modeled as an example of a highly anisotropic plate. The equivalent bulk properties used for computing dispersion curves are listed in Table III. As for the cross-ply case, all three fundamental modes are excited in certain directions. Figures 7(a) and 7(b) show snapshots of the out-of-plane surface displacement obtained from the FE model 25 μs after the start of the input signal for the anti-symmetric (A_0) and symmetric modes (S_0 and SH_0), respectively. Figures 7(c) and 7(d) show the equivalent results obtained from the asymptotic model. The fiber direction in all cases is aligned with the x axis. The agreement in all cases is good with the exception of an obvious discontinuity in the symmetric modes predicted by the asymptotic model. Figures 7(e) and 7(f) show the symmetric modes predicted by the asymptotic model separated into the contributions from the S_0 and SH_0 modes, respectively. From Fig. 7(f) it is clear that the discontinuity is again due to the SH_0 mode and that in fact two discontinuities occur at the ends of the angular range over which the SH_0 mode is excited. Between these angles, the mode again has multiple components as in the case of the cross-ply plate.

D. In-plane excitation of isotropic plate

The final example is chosen to illustrate the nonaxisymmetric field excited by an in-plane point force applied to an isotropic aluminium plate. The force is orientated at 30° to the x axis and the resulting in-plane radial, in-plane angular and out-of-plane surface displacements predicted by the asymptotic model 25 μs after the start of the input signal are shown in Figs. 8(a)–8(c), respectively. There is no accompanying FE validation in this case as the lack of symmetry requires a model with too many degrees of freedom to run on the available computer resources.

The in-plane radial and out-of-plane displacement components in this example are due entirely to the Lamb modes, A_0 and S_0, while the in-plane angular displacement is due entirely to the SH_0 mode. The modal amplitude as a function of angle with respect to the forcing direction is either sinusoidal for the SH_0 mode (i.e., maximum amplitude at right angles to forcing direction) or co-sinusoidal for the A_0 and S_0 Lamb wave modes (i.e., maximum amplitude in line with the forcing direction).

This example also illustrates a minor implementation challenge. The excitability matrices are only computed over an angular range from 0° to 90° to save time but excitability matrices may be required at any angle and a procedure is therefore required to map the available data to the desired angle. This procedure, while simple in principle, proved surprisingly awkward to implement correctly due to the need to preserve the correct sign of all nine elements in the excitability matrix in all four angular quadrants. The results in Fig. 8 show that the implementation is successful. There is continuity of all three displacement components between quadrants and the displacement components are of opposite sign on either side of the null direction for each mode.

VI. CONCLUSION

A mathematical basic of a far-field asymptotic technique for predicting the modal amplitude of the 3D guided wave field due to a harmonic point force applied to the surface of a planar multilayered anisotropic waveguide has been described. The amplitude of the displacement fields of each mode is related to the input force by modal excitability matrices which are functions of direction and frequency. A key attribute of the technique is that the excitability matrices in the 3D case are computed from the excitability matrices for the 2D case of straight-crested waves excited by line sources. The latter are readily obtained from modal dispersion data that can be computed by a number of existing methods. The numerical implementation of the technique has been discussed and practical challenges highlighted. Example results from a number of test cases have been presented which show generally good agreement with 3D time-marching finite element simulations. The points where the asymptotic assumptions are invalid are clearly visible in these results and relate to the points where the normal to the phase slowness surface of a mode (i.e., the group velocity direction) is stationary. In principle a more accurate asymptotic approximation at the vicinity of these points could be obtained but this has not yet been implemented.

[1] S. Lih and A. K. Mal, "On the accuracy of approximate plate theories for wave field calculations in composite laminates," Wave Motion **21**, 17–34 (1995).

[2] M. J. S. Lowe, "Matrix techniques for modeling ultrasonic waves in multilayered media," IEEE Trans. Ultrason. Ferroelectr. Freq. Control **42**, 525–542 (1995).

[3] L. Wang and S. I. Rokhlin, "Stable reformulation of transfer matrix method for wave propagation in layered anisotropic media," Ultrasonics **39**, 413–424 (2001).

[4] L. Gavric, "Computation of propagative waves in free rail using a finite element technique," J. Sound Vib. **185**, 531–543 (1995).

[5] T. Hayashi, W.-J. Song, and J. L. Rose, "Guided wave dispersion curves for a bar with an arbitrary cross-section, a rod and rail example," Ultrasonics **41**, 175–183 (2003).

[6] B. Pavlakovic, M. Lowe, D. Alleyne, and P. Cawley, "Disperse: A general purpose program for creating dispersion curves," in *Review of Progress in Quantitative NDE*, edited by D. Thompson and D. Chimenti (Plenum, New York, 1997), Vol. **16**, pp. 185–192.

[7] E. Glushkov and N. Glushkova, "Blocking property of energy vortices in elastic waveguides," J. Acoust. Soc. Am. **102**, 1356–1360 (1997).

[8] W. A. Green and E. R. Green, "Elastic waves in fiber composite laminates," Ultrasonics **38**, 228–231 (2000).

[9] A. J. Niklasson and S. K. Datta, "Transient ultrasonic waves in multilayered superconducting plates," J. Appl. Mech. **69**, 811–818 (2002).

[10] M. Veidta, T. Liub, and S. Kitipornchai, "Modeling of lamb waves in composite laminated plates excited by interdigital transducers," NDT & E Int. **35**, 437–447 (2002).

[11] B. A. Auld, *Acoustic Fields and Waves in Solid*, 2nd ed. (Krieger, Malabar, FL, 1990).

[12] J. J. Ditri and J. L. Rose, "Excitation of guided waves in generally anisotropic layers using finite sources," J. Appl. Mech. **61**, 330–338 (1994).

[13] V. A. Babeshko, E. V. Glushkov, and N. V. Glushkova, "Energy vortices and backward fluxes in elastic waveguides," Wave Motion **16**, 183–192 (1992).

[14] A. Mal, "Elastic waves from localized sources in composite laminates," Int. J. Solids Struct. **39**, 5481–5494 (2002).

[15] J. D. Achenbach and Y. Xu, "Wave motion in an isotropic elastic layer generated by a time harmonic point load of arbitrary direction," J. Acoust. Soc. Am. **106**, 83–90 (1999).

[16] O. Diligent and M. J. S. Lowe, "Reflection of the S_0 lamb wave mode from a flat bottom circular hole," J. Acoust. Soc. Am. **118**, 2869–2879 (2005).

[17] D. E. Chimenti, "Guided waves in plates and their use in materials characterization," Appl. Mech. Rev. **50**, 247–284 (1997).

[18] J. J. Ditri, A. Pilarski, B. Pavlakovic, and J. L. Rose, "Generation of guided waves in a plate by axisymmetric normal surface loading," in *Review of Progress in Quantitative NDE*, edited by D. Thompson and D. Chimenti (1994), Vol. **13**, pp. 133–140.

[19] P. Wilcox, "Modeling the excitation of Lamb and SH waves by point and line sources," in *Review of Progress in Quantitative NDE*, edited by D. Thompson and D. Chimenti (AIP, New York, 2004), Vol. **23**, pp. 206–213.

[20] E. Moulin, S. Grondel, M. Baouahi, and J. Assaad "Pseudo-3D modeling of a surface-bonded Lamb wave source," J. Acoust. Soc. Am. **119**, 2575–2578 (2006).

[21] I. Núñez, R. K. Ing, C. Negreira, and M. Fink "Transfer and Green functions based on modal analysis for Lamb waves generation," J. Acoust. Soc. Am. **107**, 2370–2378 (2000).

[22] E. R. Green and W. A. Green, "A computational method for wave propagation from a point load in anisotropic material," Ultrasonics **38**, 262–266 (2000).

[23] S. Banerjee, W. Prosser, and A. Mal, "Calculation of the response of a composite plate to localized dynamic surface loads using a new wave number integral method," J. Appl. Mech. **72**, 18–24 (2005).